

Assessment of Primary Frequency Control through Battery Energy Storage Systems

F. Arrigo^{a,*}, E. Bompard^a, M. Merlo^b, F. Milano^c

^a*Department of Energy, Politecnico di Torino, Corso Duca degli Abruzzi 24, Turin, Italy*

^b*Department of Energy, Politecnico di Milano, Via La Masa 34, Milan, Italy*

^c*School of Electrical and Electronic Engineering, University College Dublin, Belfield, Ireland*

Abstract

This article focuses on the impact of the primary frequency control that can be provided by Battery Energy Storage Systems (BESSs) on the transient response of electric grids. A procedure based on the Fourier transform is used for synthesizing a realistic frequency signal based on the variations of load consumption and generation. The impact of BESSs is evaluated with respect to the storage capacity installed and the regulation strategy adopted and then compared with the regulation provided by conventional sources. The impact of a variable-droop strategy on the dynamic response of the grid and the BESSs State of Charges (SOCs) is also evaluated. A novel index to quantify the performance of the BESSs is proposed and discussed. The case study is based on a detailed dynamic model of the all-island Irish transmission system.

Keywords: Battery energy storage systems, Fourier transform, frequency control, renewable energy.

1. Introduction

1.1. Motivations

The recent successful operation of a 100 MW BESS installed in South Australia indicates that BESSs are very well suited for Primary Frequency Control (PFC) due to their fast response [1]. In several European systems, BESSs

*Corresponding author

Email address: francesco.arrigo@polito.it (F. Arrigo)

6 already participate to the PFC service [2] and National Grid in UK has started
7 a new service called “enhanced frequency response” that requires a power re-
8 sponse in less than 1 second [3]. This paper addresses the open question of
9 how to assess the performance of BESSs that provide PFC compared to con-
10 ventional primary frequency controllers during normal grid dynamic conditions.
11 Such an appraisal appears particularly relevant if ancillary services are rewarded
12 proportionally to their effectiveness, as recently recommended by FERC [4].

13 *1.2. Literature Review*

14 There are several studies on the impact of BESSs on primary frequency con-
15 trol. The contribution of BESSs to frequency stability after a contingency is
16 discussed in [5, 6, 7, 8, 9]. The use of BESSs to regulate the frequency within
17 a microgrid is studied in [10, 11]. A third group of studies focuses only on the
18 BESSs without considering their impact on the grid. In these works various
19 strategies, e.g. variable droop, energy arbitrage and participation to balancing
20 markets, are utilised in order to optimize BESS profit and SOC management in
21 addition to frequency regulation. In [12, 13, 14], BESSs regulate their SOC by
22 considering the instantaneous frequency. BESS power output can be adjusted
23 using a different droop or changing the set point when the frequency is in the
24 deadband [?]. A heuristic methods or fuzzy control logic is used to control the
25 BESS response [?]. Moreover the use of market schedules and participation in
26 intra-day and balancing markets is considered to avoid over and under charging
27 values and to perform energy arbitrage [?]. More efficient approaches consider-
28 ing dynamic programming are used in [15, 16]. Multi-services provision [17] and
29 the presence of other resources like loads or PV is studied in [18, 19] by using
30 optimization approaches (e.g. model predictive control) in order to maximize
31 the frequency reserve capacity of the BESS. In UK and Central Europe, BESSs
32 are already allowed to vary their droop from the nominal value to partially
33 regulate their SOC [3, 13] by considering a small deviation from the nominal
34 point [12]. Since BESSs capacity devoted to provide PFC service to the grid is
35 expected to increase [1], Variable Droop (VD) strategies are thus expected to

36 play a relevant role.

37 Multi-hour/day simulations to study the BESSs impact on the grid are con-
38 sidered in [20, 21, 22, 23, 24]. In [20], the impact of a BESS on a small power
39 system is evaluated with field tests by changing the parameters of PFC. The
40 improvement of the frequency signal is estimated by computing the grid fre-
41 quency standard deviation when BESS is on or off, but not explicitly simulated.
42 In [21], a specific control algorithm that takes into account droop control and
43 SOC management for the BESS is implemented and its effect on the frequency
44 signal is simulated. However, no index is used to quantify this improvement.
45 In [22, 23, 24], the focus is on secondary frequency control, where BESSs are
46 introduced in the simulations to improve the stability of the grid, and their
47 performance is compared to Conventional Generation (CG).

48 The evaluation of the performance of the frequency control through BESSs
49 is closely linked to the creation of realistic frequency scenarios. In [22, 23, 24],
50 measurement data from several load profiles and photovoltaic power plants are
51 used, while the power exchanged at the tie lines and frequency reserves are
52 estimated. These approaches cannot guarantee a realistic signal, unless a huge
53 and diversified database of measurements is used, which is impractical for large
54 scale power systems. In [21], a system equivalent model is used to reproduce a
55 recorded frequency signal only if real time grid data parameters and variables
56 can be accurately estimated.

57 The definition of realistic scenarios requires a precise characterization of all
58 components and controllers of the grid. A taxonomy of the frequency variations
59 in Europe is presented in [25]. These are divided into: (i) stochastic frequency
60 deviations due to the fast variations of loads and renewable sources, (ii) deter-
61 ministic frequency deviations caused by the ramps of CG following their market
62 scheduling [26]. CG undergoes an hourly or sub-hourly unit commitment, which
63 leads to a long term mismatch with respect to the net load [27]. In order to
64 reproduce a realistic signal it is necessary to simulate both typologies of fre-
65 quency deviations and verify the resulting variability of the frequency signal
66 with real-world data.

67 *1.3. Contributions*

68 The contributions of this paper are as follows:

- 69 • quantify the impact of the primary frequency control provided by BESSs
70 and compare it to CG contribution through the use of a novel quantitative
71 index. It is also studied the impact of a VD control strategy used by
72 BESSs.
- 73 • a novel procedure, whose preliminary version appeared in [28], to generate
74 realistic synthetic frequency scenarios.

75 *1.4. Organization*

76 The remainder of the paper is organized as follows. Section 2 presents the
77 stochastic models included in the grid, whereas Section 3 describes the adopted
78 frequency control of the BESS. Section 4 outlines the procedure to create real-
79 istic scenarios. Section 5 describes various indexes, included the proposed one,
80 to evaluate the performance of the control provided by BESSs and other energy
81 resources. Section 6 describes the case study and discusses simulation results.
82 Finally, Section 7 provides conclusions and outlines future work.

83 **2. Modelling of Stochastic Processes**

84 In normal dynamic conditions, frequency variations are mostly determined
85 by the unbalance between total produced and consumed power [29]. This un-
86 balance is caused by the variations of loads, wind power plants and conventional
87 generators ramping to change set point. Power variations are stochastic and,
88 thus, a proper mechanism to emulate randomness has to be put in place to
89 obtain realistic results from simulations. We provide below a short description
90 of the devices involved in the creation of the power disturbances considered in
91 this work.

92 *2.1. Conventional Generation*

93 The PFC of conventional power plants is shown in Fig. 1. f_{nom} is the nominal
 94 frequency of the grid, while f is the instantaneous frequency value, p_{pfc} is the
 95 power requested by primary frequency control, p_{ord} is the power reference set
 96 point of the turbine and R [pu(Hz)/pu(MW)] is the droop of the controller.
 97 The lead-lag block represents the turbine governor dynamics and p_m is the
 98 mechanical output of the turbine. By changing the time constants it is possible
 99 to simulate different CG technologies like steam, gas and hydro power plants.
 100 The model is detailed enough for transient stability studies, where frequency
 101 variations remain well bounded and the focus is the overall response of the
 102 system. As explained in Section 4, p_{ord} is subjected to ramps of maximum
 103 amplitude $|\Delta p_{\text{max}}|$ with time period Δt_{CG} ranging from few minutes up to
 104 one hour in order to mimic the power variations yielded by net load following
 105 dispatching. In such a way, we reproduce slow power fluctuations around the
 106 net load. An example of such fluctuations is shown in Fig. 2.

107 *2.2. Load*

Load models are assumed to be voltage-dependent, i.e., exponential or ZIP
 models, and either static or dynamic voltage recovery [30]. The reference power
 consumption of a load, say p_{load} , is defined as the sum of two components:

$$p_{\text{load}} = p_{\text{det}} + p_{\text{sto}} , \quad (1)$$

108 where p_{det} is the “deterministic” consumption which is assumed to vary linearly
 109 between assigned values in a given period, e.g. 15 minutes; p_{sto} is a stochastic

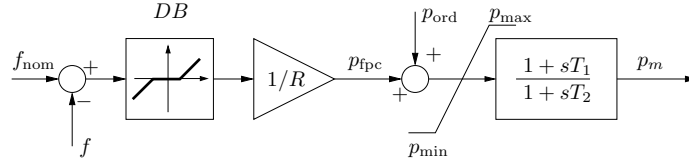


Figure 1: Simplified model of the primary frequency control and turbine of conventional power plants. Note that all quantities in the figure are in pu.

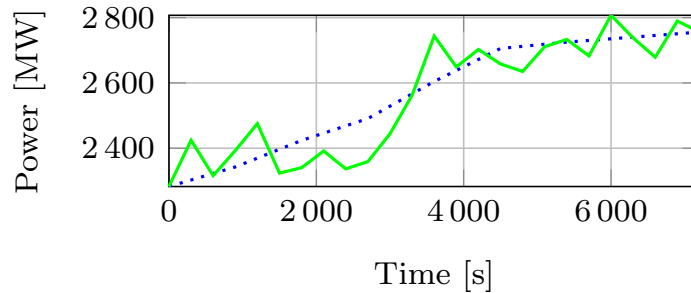


Figure 2: Example of noise that reproduces slow fluctuations. The blue dotted line represents the net load, while the green solid line represents the net load plus CG fluctuations.

110 fluctuation that models volatility. p_{sto} is defined as a Gaussian distribution
 111 with a given standard deviation σ_{Load} . Stochastic variations are computed with
 112 a given period Δt_i . Fig. 3 shows an example of load profiles.

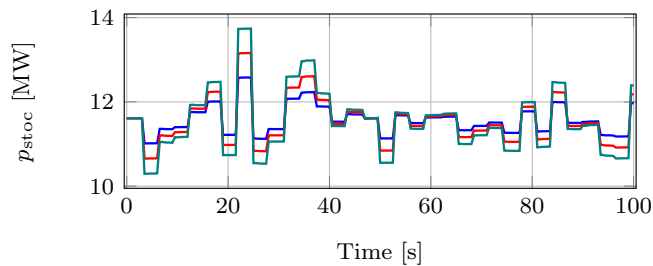


Figure 3: Examples of p_{sto} profiles using $\Delta t_i = 3$ s and various standard deviations, namely 2.5, 4 and 5.5%.

113 *2.3. Wind Generation*

Wind generators are modelled as doubly-fed induction generators (Type C). The turbine is fed by wind speed time series, which are defined as the sum of two components: wind speed stochastic component $w_{\text{s,sto}}$ [m/s] and $w_{\text{s,ramp}}$ [m/s] component modelled as linear wind speed ramps with a certain time period. The stochastic component is modelled as a set of Stochastic Differential Equations (SDEs) based on the Ornstein-Uhlenbeck Process [31], also known as mean-

reverting process. The equations for the wind speed ω_s can be written as follows:

$$w_s = w_{s,\text{ramp}} + w_{s,\text{sto}} , \quad (2)$$

$$\dot{w}_{s,\text{sto}} = \alpha(\mu_w - w_{s,\text{sto}}) + b_w(\sigma_w)\xi_w , \quad (3)$$

114 α is the mean reversion speed that dictates how quickly the $w_{s,\text{sto}}$ tends to the
 115 given mean value μ_w (in our case 0). ξ_w is the white noise, formally defined
 116 as the time derivative of the Wiener process. This process is controlled by
 117 adjusting α and the standard deviation σ_w of the wind stochastic part which
 118 affects the b_w component. Fig. 4 shows three sample wind stochastic profiles
 119 obtained by changing the σ_w and α parameter.

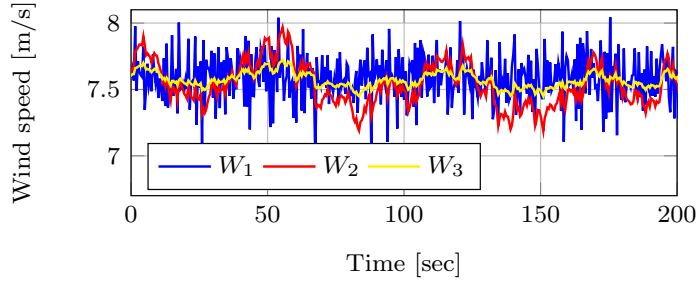


Figure 4: $w_{s,\text{sto}}$ profiles. W_1 ($\alpha = 10$, $\sigma_w = 0.17$); W_2 ($\alpha = 0.1$, $\sigma_w = 0.17$); W_3 ($\alpha = 0.1$, $\sigma_w = 0.06$).

120 3. BESS Control

121 In this study, we consider the BESS model defined in [32]. The power pro-
 122 duced by the battery is transferred to the grid through a current source con-
 123 verter. The converter includes the PI controllers that regulate the active and
 124 reactive powers at the point-of-connection with the ac grid. Overall the BESS
 125 responds within a second after a Δp request. The reference active power is
 126 defined by the PFC control. Two PFC characteristics are considered in this
 127 study, namely fixed and variable droop control strategy. The latter is a novel
 128 contribution of this paper.

129 *3.1. Fixed Droop (FD)*

This control is implemented as a fixed power/frequency curve, as commonly in use for CG. The droop (R) of CG plants is usually set at 0.04 or 0.05 pu considering a 10% regulation band of the generator nominal power, as specified in the Irish grid code [33]. Depending on these parameters, a certain frequency error Δf_{\max} causes the full provision of the regulation band. In general the droop for a CG and a BESS unit is computed as follows [34]:

$$R_{\text{CG}} = \left| -\frac{\Delta f_{\max}}{f_{\text{nom}}} \cdot \frac{1}{PFC_{\text{band}}^{\text{CG}}} \right|, \quad (4)$$

$$R_{\text{BESS}} = \left| -\frac{\Delta f_{\max}}{f_{\text{nom}}} \cdot \frac{1}{PFC_{\text{band}}^{\text{BESS}}} \right|, \quad (5)$$

where PFC_{band} represents the regulator band in pu (in this study, we set $PFC_{\text{band}}^{\text{CG}} = 0.1$ pu(MW) and $PFC_{\text{band}}^{\text{BESS}} = 1$ pu(MW)). Taking Δf_{\max} equal for both resources and dividing equation (5) by (4), we obtain the relationship which correlates both the droops:

$$R_{\text{BESS}} = R_{\text{CG}} \cdot \frac{PFC_{\text{band}}^{\text{CG}}}{PFC_{\text{band}}^{\text{BESS}}} = R_{\text{CG}} \cdot 0.1. \quad (6)$$

130 For each value of the CG droop one obtains a corresponding BESS droop
 131 which saturates its regulation band at the same frequency deviation of the CG
 132 resources.

133 *3.2. Variable Droop (VD)*

134 Frequency fluctuations distribute symmetrically around f_{nom} and follow a
 135 normal distribution or a binomial one if a deadband in governors controller of CG
 136 is present [35]. Therefore, the PFC of the battery usually works on average 50%
 137 in under-frequency and 50% over-frequency periods with a zero mean energy.
 138 However, using a FD frequency control characteristic, due to the internal losses
 139 of the battery the SOC is expected to gradually decrease to 0. At the same
 140 time, long over-frequency periods could make the BESS reach maximum SOC,
 141 limiting its regulation capacity. The proposed VD strategy tries to avoid such
 142 extreme SOC conditions by introducing an asymmetry in the frequency control
 143 of the BESS.

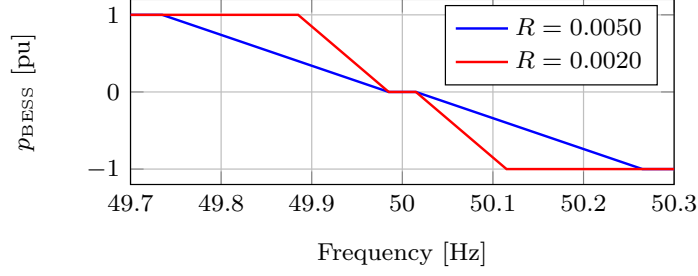


Figure 5: Power limits example for the VD frequency control.

		Low SOC_i → High SOC_i				
		SOC_1	...	SOC_{ave}	...	SOC_n
↑ $\Delta f_{e,j} > 0$ $\Delta f_{e,j} < 0$ ↓	$\Delta f_{e,1}$	$R_{1,1}$...	R_{ave}	...	$R_{n,1}$
	\vdots	\vdots		\vdots		\vdots
	$\Delta f_{e,m}$	\vdots		\vdots		\vdots
	$\Delta f_{e,m+1}$	\vdots		\vdots		\vdots
	\vdots	\vdots		\vdots		\vdots
	$\Delta f_{e,2m}$	$R_{1,2m}$...	R_{ave}	...	$R_{n,2m}$

Figure 6: VD lookup table scheme.

144 As shown in Fig. 5, we assume that the droop is variable and bounded by two
145 values, namely R_{max} and R_{min} . These values are limited by system stability and
146 resources technical considerations. Usually TSOs request droop values between
147 2 and 8% [36], typical values are 4 and 5%.

148 The VD is implemented through the use of a two dimensional lookup table,
149 where the droop value depends on the instantaneous frequency error $\Delta f_e =$
150 $f_{nom} - f$ and the SOC. The droop values are divided in five different areas (see
151 Fig. 6): (i) in the red areas the values are close to R_{max} , (ii) in the blue areas
152 the values are close to R_{min} and (iii) in the green area (which correspond to
153 a column vector) the droop values are all equal to the average droop R_{ave} , at
154 half distance between R_{max} and R_{min} . The values of the table are therefore
155 constructed symmetrically in such a way that the BESS is expected to avoid

156 excess discharge or charge keeping its SOC close to SOC_{ave} level. As an example,
157 if SOC is high and Δf_e is positive then the BESS discharges with a low droop
158 to reach SOC_{ave} , whereas if Δf_e is negative it charges with a high droop to slow
159 down the SOC increase.

160 Note that, in order to regulate the SOC the best choice would be to set
161 the droop values equal to R_{max} in red areas and R_{min} in blue areas. However,
162 to avoid sudden droop changes and less effective frequency regulation, droop
163 values gradually approach R_{max} and R_{min} .

164 A better SOC regulation is achieved by setting the SOC_i values close to
165 SOC_{ave} and taking small values of $\Delta f_{e,j}$. Better SOC management is also
166 expected if the distance between the maximum and minimum droop R_{max} and
167 R_{min} is large.

168 The VD strategy here proposed cannot achieve a perfect SOC regulation
169 being a decentralized technique, nevertheless it is useful to improve the SOC
170 dynamics with respect to a FD strategy and it is used in this study to make the
171 BESS droop change realistically during the simulations and analyse the impact
172 of VD strategies on the grid frequency stability.

173 4. Generation of Realistic Scenarios

174 Our aim is now to reproduce realistic frequency fluctuations in order to
175 properly quantify the BESS contribution to the PFC. The reference scenario,
176 considered below, is a time series of the frequency measured by the authors at
177 University College of Dublin. The data represents 330 days of measurements
178 with a sampling rate of 10 Hz.

179 A Discrete Fourier Transform (DFT) is applied to define the harmonic con-
180 tent of the frequency measurements. The goal is to synthesize and then simulate
181 a dynamic base case scenario (S1) with a harmonic content similar to the real
182 frequency data sampled in the lab. The implemented procedure is valid to
183 replicate the harmonic amplitudes of six hours of real frequency signal. Of all
184 the thousands of harmonics computed through the DFT, only the first 800 are

185 considered, which represent more than the 98% of the variance of the signal for
 186 all the days considered (as computed by applying Parseval’s Theorem). The
 187 frequency signal is therefore a ”slow” signal in that the first harmonics (charac-
 188 terized by longer periods) hold more importance than the shorter period ones.
 189 For example, in Fig. 7 we show the harmonic profiles related to the six hour pe-
 190 riod going from 6:00 to 12:00, the mean μ and the standard deviation σ of each
 191 harmonic for all days considered. All the profiles are similar. The grid frequency
 192 signal is therefore quite variable in time domain but much more similar in the
 193 harmonic content. Therefore, to reproduce similar harmonic amplitudes of the
 194 real data assures that the synthetic signal behaves realistically. Similar results
 195 hold for the other three time ranges (00:00-6:00, 12:00-18:00, 18:00-24:00).

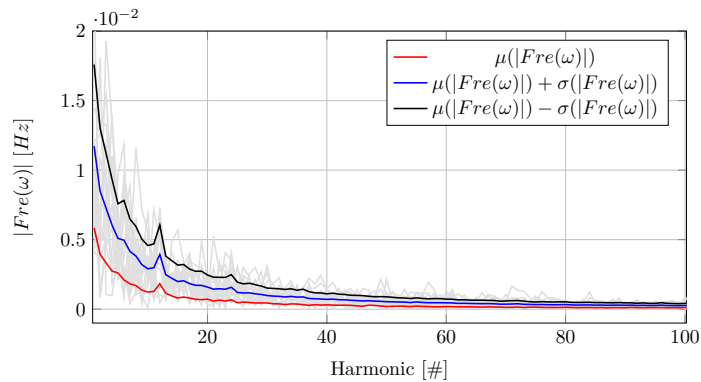


Figure 7: Harmonics amplitudes related to the six hour period 6:00-12:00.

196 In order to reproduce real data harmonics, we make use of power stochastic
 197 profiles from generation and consumption. These processes are divided in two
 198 groups following the taxonomy presented in the literature review, as follows:

- 199 • *Fast Stochastic Processes (FSP)*. The stochastic processes of load con-
 200 sumption and wind speed discussed in Section 2 are used to replicate the
 201 events that cause stochastic frequency fluctuations in the grid (typically
 202 with period lower than 2 minutes).
- 203 • *Slow Stochastic Processes (SSP)*. Two noises are used to model determin-

204 stochastic frequency deviations: SSP1 which models wind and CG ramps and
 205 SSP2 which models the long term mismatch between net load and con-
 206 ventional generation due to the market structure of the system. SSP1 are
 207 noises up to 10 minutes, while SSP2 are up to one hour. We refer to these
 208 deviations as slow frequency variations.

209 To tune the parameters of each component of FSP and SSP, a precise map-
 210 ping between stochastic processes and excited frequency harmonics is defined
 211 and stored in a database. This is obtained by varying the parameters values,
 212 simulating the grid and then computing and recording the resulting harmonic
 213 amplitude. To separate the effect of each stochastic process, one perturbation at
 214 a time is considered, being null all other stochastic processes. The parameters
 215 used to variate the stochastic processes are the ones described in Section 2 and
 216 are a total of 7.

217 In particular, for the load model, a variety of time periods Δt_i (going from
 218 0.5 to 2 seconds) and standard deviations σ_{Load} (going from 2 to 15%) values
 219 are considered. σ_w is the only parameter to be changed to vary the stochasticity
 220 of the wind component with α fixed to 0.1. For the SSP, time steps and power
 221 ramps are chosen from uniform distributions with specified limit values. In the
 222 case of SSP1, time steps Δt_{CG} go from 2 to 10 minutes, while for SSP2 the
 223 period goes from 13 to 60 minutes. In the case of power variations, requested
 224 ramps are both negative or positive, with a maximum $|\Delta p_{\text{max}}|$ which goes from
 225 10 MW up to 70 MW for both SSP noises.

226 Figures 8 and 9 show several harmonic profiles obtained from the simulation
 227 of FSP and SSP noises. As expected, The former noises excite short period
 228 harmonics, while the latter give rise exclusively to long period harmonics.

 Finally, the stochastic processes of loads, wind speeds and CG power set
 points are summed together and the resulting profile, say p_{tot} , is thus identified
 by a given unique set of parameters that define the four stochastic processes.
 The harmonic contents of the frequency trajectories obtained with p_{tot} are then
 compared with the real data through the estimation of an error ϵ_f , which is

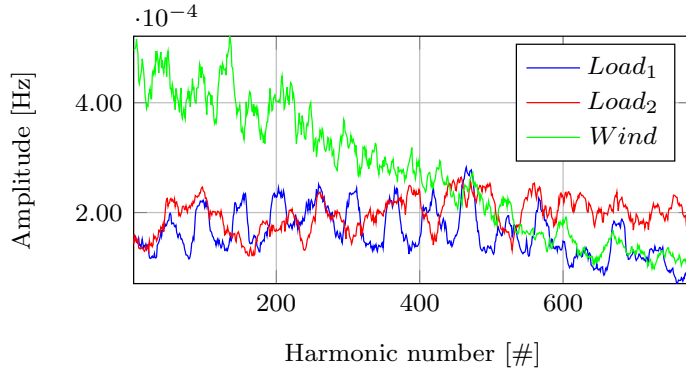


Figure 8: Examples of harmonic obtained with load and wind stochastic processes. $Load_1$ ($\Delta t_i = 1s$, $\sigma_{Load} = 2\%$); $Load_2$ ($\Delta t_i = 0.5s$, $\sigma_{Load} = 2\%$); Wind ($\sigma_w = 3\%$).

defined as follows:

$$\epsilon_i = \begin{cases} |(Y_{sim_i} - (Y_{real_i} - std_i))|, & \text{if } Y_{sim_i} < (Y_{real_i} - std_i), \\ (Y_{sim_i} - (Y_{real_i} + std_i)), & \text{if } Y_{sim_i} > (Y_{real_i} + std_i), \\ 0, & \text{if } (Y_{real_i} - std_i) < Y_{sim_i} < (Y_{real_i} + std_i) \end{cases} \quad (7)$$

$$\epsilon_f = \frac{\sum_{i=1}^{N_{harm}} \epsilon_i}{\sum_{i=1}^{N_{harm}} Y_{real_i}} \quad (8)$$

229 where ϵ_i is the error at the harmonic i ; Y_{sim_i} is the value of the simulated
 230 frequency data at the harmonic i ; Y_{real_i} is the mean of all real data at the
 231 harmonic i ; std_i is the standard deviation of the real frequency data at the
 232 harmonic i ; N_{harm} is the number of harmonic used.

233 If this error falls within the desired tolerance, the procedure ends, otherwise
 234 relevant noise parameters are increased or decreased according to their impact
 235 on the signal harmonics. In such a way the procedure creates a scenario in which
 236 frequency does not emulate a specific real day data, but it tries to recover the
 237 average variability of real measurements. The synoptic scheme that illustrates
 238 the procedure is shown in Fig. 10.

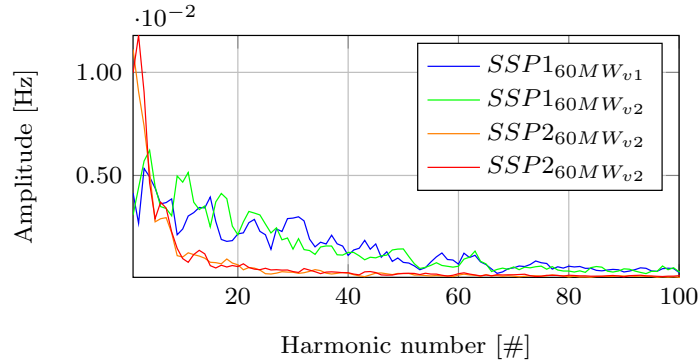


Figure 9: Examples of harmonic groups obtained with the SSP1 and SSP2 noises. $v1$ and $v2$ refer to different noise profiles with equal $|\Delta p_{\max}|$ value. Δt_{CG} is equal to 3-7 minutes for SSP1 and 13-50 minutes for SSP2.

239 5. Indexes

240 This section describes a variety of indexes that allow evaluating the impact
 241 of stochastic processes and the effectiveness of the PFC provided by BESSs and
 242 CG.

243 5.1. Impact of the stochastic processes on the system dynamic response

To quantify the contribution of each stochastic process to the overall frequency fluctuations, we consider the sum variance law of the frequency signal which defines the variance of a signal composed by N stochastic independent variables as:

$$\sigma_{\text{TOT}}^2 = \sum_{i=1}^N \sigma_i^2 . \quad (9)$$

To compare the impact of each process, it is convenient to consider a normalized variance per process, namely:

$$\sigma_{i,\text{pu}}^2 = \frac{\sigma_i^2}{\sigma_{\text{TOT}}^2} , \quad (10)$$

in such a way, from Equ. (9), we can write:

$$1 = \sum_{i=1}^N \sigma_{i,\text{pu}}^2 . \quad (11)$$

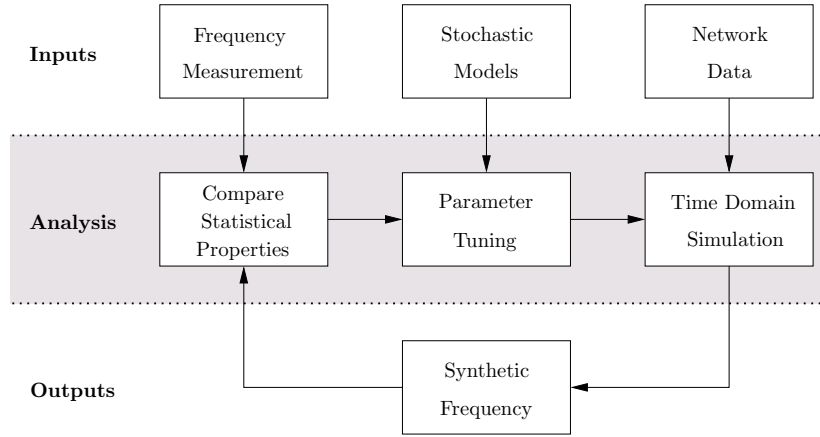


Figure 10: Procedure to generate realistic scenarios.

244 *5.2. Impact of BESSs on frequency fluctuations*

This index provides a measure of the relative improvement to the dynamics response due to the BESSs. It is defined as:

$$h_B = 1 - \frac{\sigma_B}{\sigma_o} , \quad (12)$$

245 where σ_B is the standard deviation of the frequency of the system with inclusion
 246 of BESSs and σ_o is the standard deviation of the frequency for the same scenario
 247 but without BESSs.

248 *5.3. Effectiveness of the PFC*

This novel proposed index evaluates the effectiveness of the frequency control provided by any resource included in the system. Considering a resource k , the index is defined as:

$$e_k = \frac{E_k^+ + |E_k^-| - (E_{o,k}^+ + |E_{o,k}^-|)}{E_k^{\text{ref}}} , \quad (13)$$

where

$$E_k^{\text{ref}} = \int_o^T \frac{P_{\text{nom},k}}{R_k(r)} |\Delta f(r)| dr . \quad (14)$$

249 R_k [pu] is the droop of the resource which, for the BESS regulated with VD, is
 250 a time-dependent quantity, $P_{\text{nom},k}$ [MW] is the nominal power of the resource

251 and $|\Delta f(r)|$ [Hz] is the frequency error including the deadband. E_k^{ref} represents
 252 the integral of the exact real-time power profile requested by the PFC service in
 253 a given period T , E_k^+ represents the actual energy produced by the resources for
 254 $\Delta f > 0$, whereas E_k^- is the energy produced for $\Delta f < 0$ in the same period T .
 255 The condition $E_k^+ + E_k^- < E_k^{\text{ref}}$ generally holds as E_k^+ and E_k^- account for the
 256 delays of the primary frequency control dynamics. $E_{o,k}^+$ and $|E_{o,k}^-|$ represent the
 257 energy produced for $|\Delta f| < db$ where db is the deadband of the controller. These
 258 energies work against the PFC requirements and thus reduce the effectiveness
 259 of the frequency control.

260 According to the above definition, $e_k = 0$ if the resource does not partic-
 261 ipate to PFC, $e_k \ll 1$ if the resource is slow and not able to follow the PFC
 262 reference signal and $e_k = 1$ for an ideal frequency control with instantaneous
 263 time response.

264 6. Case Study

265 This case study discusses the performance of the BESS PFC described in
 266 Section 3 and its impact on various scenarios based on the procedure discussed
 267 in Section 4. With this aim, we make use of the Irish transmission system [37].
 268 Table A.5 in the appendix summarizes the main elements of the grid. The CG
 269 active installed capacity in S1 is 4347 MW while wind active installed capacity
 270 is 2123 MW. In S2 and S3 CG capacity is decreased by 25%.

271 All simulations are solved using Dome [38], a Python and C-software based
 272 tool that allows simulating large scale power systems modelled as a set of
 273 stochastic differential algebraic equations. Relevant components are modelled
 274 in detail such as a high voltage network topology, a 6-th order machine model
 275 of the synchronous generator, frequency and voltage regulators etc.

276 6.1. Scenarios Construction

277 Three scenarios, S1, S2 and S3, are considered. In Appendix A we report
 278 the static and dynamic parameters of the CG PFC.

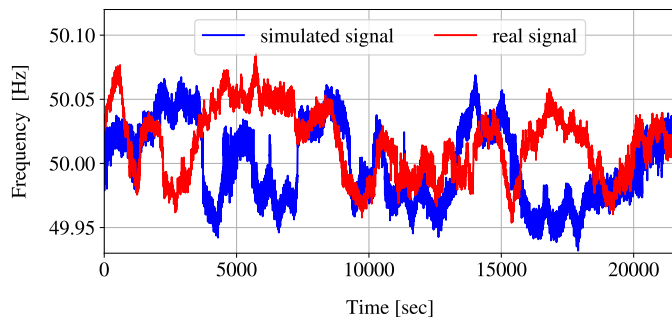


Figure 11: Comparison between real and simulated (S1) frequency

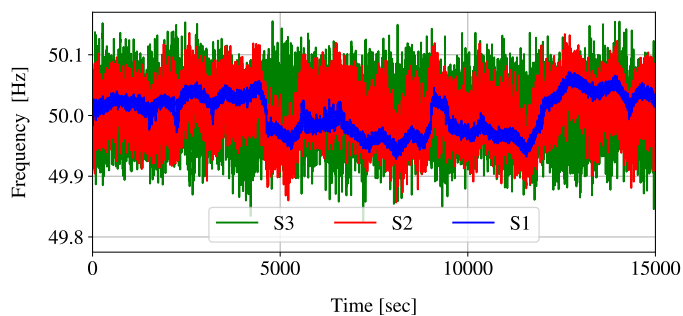


Figure 12: Frequency profiles examples for the three considered scenarios.

279 The time horizon of the three scenarios is 12 hours, from 6:00 to 18:00.
 280 Load and wind linear slow power profiles are defined based on real-world data
 281 obtained by the Irish TSO Eirgrid, while the mismatch from the net load comes
 282 from the application of the 4 noises presented in Section 4.

283 Each scenario is first simulated without the BESSs. S1 represents the sce-
 284 nario that reproduces the measurement data obtained in the lab. S2 and S3
 285 include higher level of noises and decreasing inertia levels, which lead to greater
 286 and faster frequency fluctuations. In particular, in S2 we increase the FSP noises
 287 and decrease the SSP2 noise, while in S3 the SSP noises are reduced almost to
 288 zero and FSP noises are highly increased.

289 One profile of scenario S1 and a real frequency time series are shown in
 290 Fig. 11. As expected, the synthetic frequency signal retains a similar variability

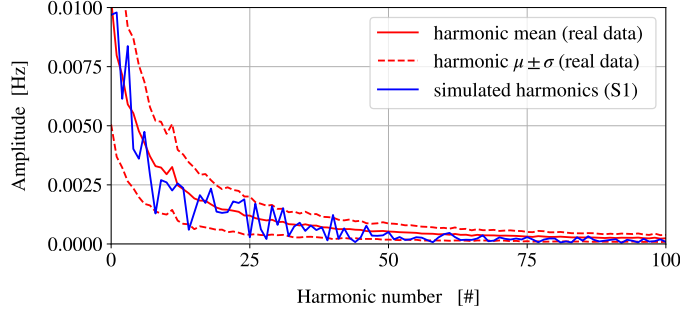


Figure 13: Harmonic comparison between simulated and real data for the scenario S1, period 12:00 - 18:00.

291 with respect to the real data. Sample frequency fluctuations of the three sce-
 292 narios are shown in Fig. 12. Table 1 summarizes the standard deviation of the
 293 frequency of the system σ_f , the normalized variances $\sigma_{i,\text{pu}}^2$ of the four stochastic
 294 components and the two S1 errors ϵ_f evaluated by applying Equ. (8). In S1
 295 (real-world scenario) the slow noises (SSP) represent almost 90% of the grid
 296 deviations with more than half coming from SSP2 noises. In S2 and S3, SSP2
 297 noise goes towards zero. The noises parameters which were used to create the
 298 scenarios can be seen in Table B.8 in Appendix B. Note that in both this table
 299 and table 1 values of S2 and S3 were computed as the average between the two
 300 six hours time periods.

301 In Fig. 7 the harmonics of real data and S1 scenario are compared and as
 302 expected from the definition of error ϵ_f , the simulated profile is well bounded by
 303 the real data harmonics standard deviation. Moreover the mean of the signal in
 304 the scenarios is set in accordance with the mean of the 330 real days. For this
 305 reason, frequency signal is slightly under 50 Hz for the first 6 hours and over 50
 306 Hz for the period from 12:00 to 18:00. These frequency mean offsets are very
 307 important in order to capture day frequency dynamics which affect the BESS
 308 SOC profiles.

Table 1: Normalized variances and frequency standard deviations for the three stochastic scenarios

Scenario #	σ_f [Hz]	μ_f [Hz]	$\sigma_{i,\text{pu}}^2$				ϵ_f [pu]
			Load	$Wind_{\text{sto}}$	SSP_1	SSP_2	
S1 (6:00-12:00)	0.0308	49.9996	0.09	0.02	0.34	0.55	0.032
S1 (12:00-18:00)	0.0302	50.0038	0.075	0.07	0.34	0.515	0.021
S2 (6:00-18:00)	0.0359	50.0028	0.22	0.12	0.37	0.29	-
S3 (6:00-18:00)	0.0431	50.0021	0.55	0.24	0.16	0.05	-

309 *6.2. BESS Frequency Control*

310 The simulations that include BESSs are divided in two groups: the first
311 considers exclusively the dynamic behaviour of FD, the second compares FD
312 and VD control strategies. For the first group, the three scenarios are simulated
313 by considering four BESS capacities (100, 200, 300 and 400 MW) and three
314 droop values ($R_{BESS} = 0.005, 0.004, 0.0035$). In the second group, S1 and S2
315 scenarios are simulated, with 100, 200 and 300 MW of BESSs characterized by
316 two efficiencies ($\eta_{BESS} = 0.8, 0.9$) and by a power-energy ratio equal to 0.4.

317 With regard to the PFC, two FD droops (equal to 0.004 and 0.0035) are
318 compared respectively to two VD strategies which are shown in Table 2: (i)
319 “hard mode”, for which the droop varies in the range $R \in [0.002, 0.005]$, and
320 (ii) “soft mode”, for which the droop varies in the range $R \in [0.003, 0.005]$. The
321 tables have been built following the process described in Section 3.2 considering
322 4 SOC_i and 4 $\Delta f_{e,j}$ points. For both modes $SOC_{\text{ave}} = 60\%$, while R_{ave} is
323 equal to 0.004 in the hard mode and 0.0035 in the soft mode which are the
324 values used by the FD strategy. Both setups, especially hard mode, make the
325 droop to vary significantly during the simulations in order to regulate the SOC
326 as well as possible.

Table 2: Lookup tables for VD “hard” and “soft” control modes. Note that droop is here expressed in % and not in pu to improve readability of values.

Hard mode					Soft mode				
Δf_e	SOC range				Δf_e	SOC range			
[Hz]	50%	55%	60%	70%	[Hz]	45%	50%	60%	75%
0.03	0.20	0.20	0.35	0.50	0.040	0.3	0.35	0.40	0.50
0.0175	0.20	0.25	0.35	0.50	0.020	0.35	0.375	0.40	0.50
-0.0175	0.50	0.45	0.35	0.20	-0.020	0.45	0.425	0.40	0.30
-0.03	0.50	0.50	0.35	0.20	-0.040	0.50	0.45	0.40	0.30

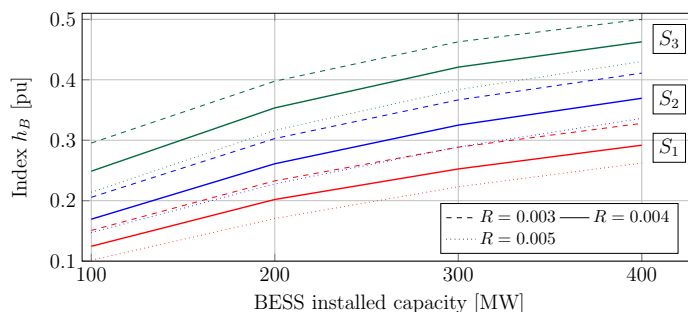


Figure 14: Index h_B for the FD control strategy of the BESSs. The droop values is indicated by R . Different colors represents different scenarios.

327 6.2.1. FD control strategy

328 Figure 14 shows the index h_B for the various scenarios. The improvement of
 329 the frequency signal is more relevant for both scenarios S2 and S3 (see Fig. 15
 330 for an example) than for S1. This has to be expected as, in S1, frequency has
 331 smaller standard deviation closer to the deadband value, which limits the impact
 332 of BESSs. For similar reasons, as shown Fig. 14, the h_B index increments tend
 333 to decrease as BESS capacity increases.

334 Table 3 shows the index e_k for the available resources that provide PFC. In
 335 the table, only one value for each scenario and each resource is shown, as e_k is

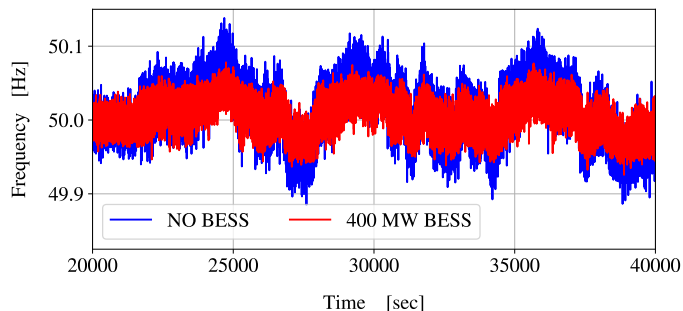


Figure 15: Frequency profiles for scenario S2 without BESS and with BESS.

Table 3: Index e_k for various scenarios and energy resources

Device	S1	S2	S3
BESS	0.99	0.99	0.97
Steam	0.92	0.78	0.31
Hydro	0.94	0.84	0.44
Gas	0.99	0.98	0.89

336 not greatly affected by the BESS installed capacity and its droop value. Two
 337 parameters mostly influence the index e_k :

- 338 • *The time response of the resource.* A fast time response of the resource
 339 improves its frequency regulation. As an example Fig. 16 shows the active
 340 power outputs of the BESS and of a conventional steam power plant.
 341 The blu dotted line is the reference PFC signal to be followed by the
 342 two resources. The fast response of the BESS leads to an almost perfect
 343 tracking of the reference signal.
- 344 • *The harmonic content of the frequency fluctuations.* The index e_k of the
 345 conventional power plants is higher in scenarios S1 and S2 than S3 in that
 346 the frequency signal is slower and easier to follow even for slower resources.

347 The result of the simulations is that in scenario S1, which represents the

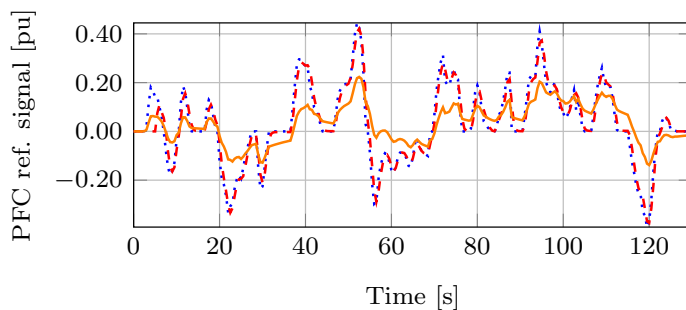


Figure 16: Power production of the BESS (dashed red line) and of CG (solid orange line) following a PFC reference signal (dotted blue line).

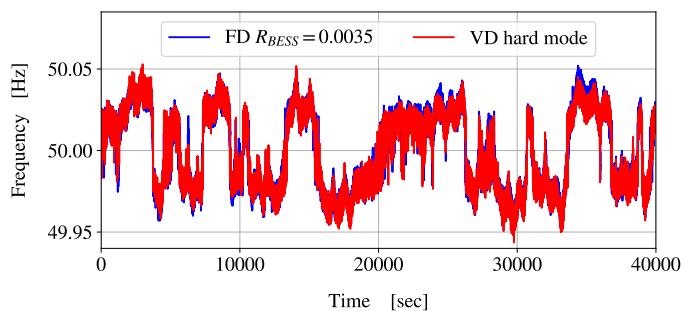


Figure 17: Frequency profiles examples with FD and VD strategy ($\eta_{\text{BESS}} = 0.8$) adopted and 200 MW BESS installed.

348 current situation, the performance of the BESSs is comparable with that of
 349 conventional power plants. In S2 and S3, which are characterized by faster
 350 frequency fluctuations, the regulation provided by BESSs have much more value
 351 than CG PFC service.

352 6.2.2. VD control strategy

353 In order to asses the impact of VD strategies, several standard statistical
 354 properties of the frequency signal are used. Note that only the results with
 355 $\eta_{\text{BESS}} = 0.8$ are shown. The cases with $\eta_{\text{BESS}} = 0.9$ provide similar results
 356 and thus are here neglected. In the case of VD strategies, the standard devia-
 357 tion of the frequency signal has a negligible difference in the order of 10^{-4} Hz

Table 4: Relevant parameters of simulations related to the case $\eta_{\text{BESS}} = 0.8$

Sim.	Par.	VD_{hard}	$FD_{0.35}$	VD_{soft}	$FD_{0.4}$
$S1_{200\text{MW}}$	$\sigma(\text{fre})$	0.0239	0.02393	0.02444	0.02443
	Skew(fre)	-0.1004	-0.0662	-0.0821	-0.722
	$\mu(\text{SOC})$	0.57	0.58	0.56	0.54
$S1_{300\text{MW}}$	$\sigma(\text{fre})$	0.0223	0.02235	0.02285	0.02286
	Skew	-0.143	-0.118	-0.122	-0.12
	$\mu(\text{SOC})$	0.59	0.61	0.59	0.62
$S2_{200\text{MW}}$	$\sigma(\text{fre})$	0.02595	0.02581	0.02655	0.02648
	Skew	0.143	0.066	0.0938	0.0722
	$\mu(\text{SOC})$	0.63	0.70	0.63	0.69
$S2_{300\text{MW}}$	$\sigma(\text{fre})$	0.02349	0.02342	0.02418	0.02416
	Skew	0.142	0.04	0.131	0.042
	$\mu(\text{SOC})$	0.63	0.66	0.63	0.64

358 with respect to the FD strategies. In Fig. 17 we can visualize the frequency
 359 signal of selected simulations which show great similarity. As shown in Table
 360 4, VD strategies generally enlarge skewness, creating small asymmetries in the
 361 frequency signal. If the initial skewness is negative, the VD strategies will fur-
 362 ther lower this value, while the opposite is true in case the initial skewness is
 363 positive. The difference is bigger in the case of hard mode with respect to soft
 364 mode and when BESS installed capacity is higher, except for the case $S1_{300MW}$.
 365 In general two compensating effects happen as BESS capacity increases: on one
 366 hand, as SOC diverges from the nominal SOC_{ave} value, the droop fluctuates
 367 around R_{ave} . This dynamic is responsible for creating the asymmetries in the
 368 frequency signal and increases its impact as more BESSs are used. On the other
 369 hand, the big BESS capacity makes the frequency less variable and closer to the
 370 deadband limiting the impact of VD strategies.

371 For these reasons the differences in the frequency signal remain small in
 372 the order of 10^{-1} [pu] and the values of skewness are still quite close to 0
 373 and therefore do not represent a big distortion. Finally, in both scenarios, the
 374 kurtosis slightly increase in the order of 10^{-3} [pu].

375 It is therefore clear that little difference exist between VD and FD strate-
 376 gies even if a large BESS capacity is installed. Both strategies are enough to
 377 guarantee stability in the grid during normal dynamic conditions.

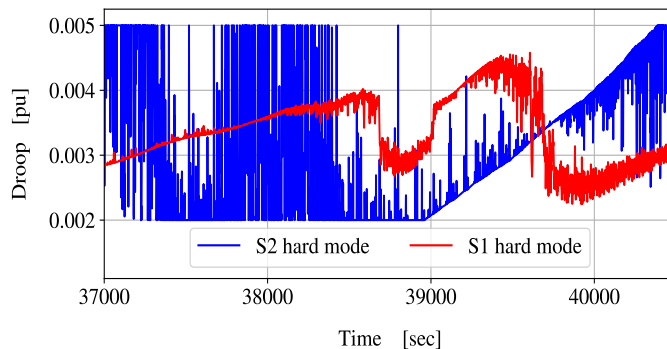


Figure 18: Example of droop profiles in S2 with 100 MW of BESS installed and $\eta_{BESS} = 0.8$

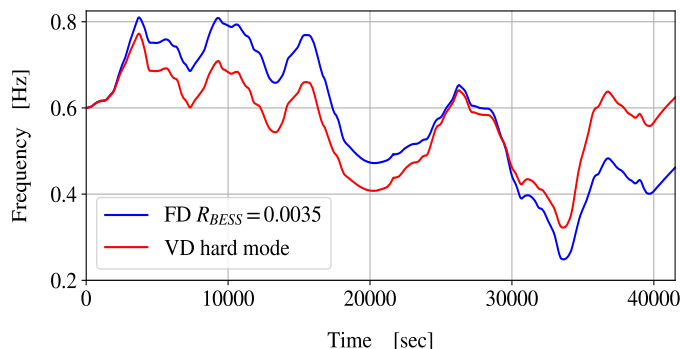


Figure 19: Example of SOC profiles in the S1 scenario with 100 MW of BESS installed

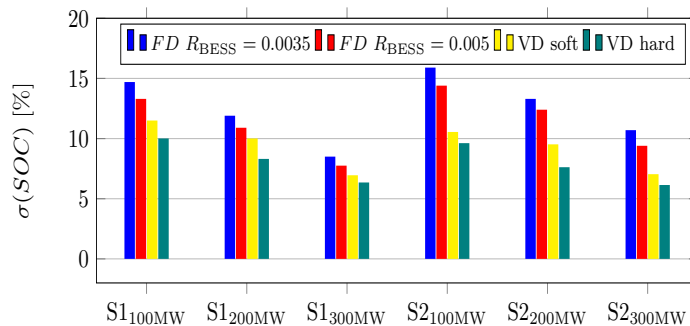


Figure 20: Index $\sigma(SOC)$ for various BESS control strategies and capacities with $\eta_{BESS} = 0.8$.

378 For what concerns SOC, in Table 4 the mean SOC value $\mu(SOC)$ of several
 379 simulations is shown. VD strategies, especially for S2, are able to keep the
 380 SOC statistically closer to SOC_{ave} with respect to FD strategies. Fig. 19 shows
 381 as an example two profiles related to the different strategies. As can be seen,
 382 the VD strategy is not able to perfectly regulate the SOC, but manages to
 383 decrease its standard deviation with respect to the FD case avoiding too high
 384 or too low charge levels. Fig. 20 shows the SOC standard deviation for all the
 385 scenarios studied in the case $\eta_{BESS} = 0.8$. The decrease in standard deviation
 386 is slightly better in S2 where the alternation between over and under-frequency
 387 periods is faster, therefore the VD strategy changes values often (as shown

388 in Fig. 18), reaching better performances. The possibility of using a bigger
389 difference between R_{\max} and R_{\min} can further improve the SOC dynamics (e.g.
390 $R_{\min} = 0.002$ and $R_{\max} = 0.008$), but its effect on the frequency must be
391 carefully evaluated.

392 7. Conclusions

393 In this paper we have studied the potential impact of BESSs on the PFC
394 of power systems. Realistic scenarios are generated through a technique that
395 properly reproduces load and generation variations based on the the DFT. Sim-
396 ulation results confirm that BESSs can reduce the fluctuations of the frequency
397 provided that they are properly controlled and enough capacity is installed. The
398 effectiveness of the frequency support is quantified by means of an effectiveness
399 index e_k .

400 The performance of the BESS control depends both on the amount of inertia
401 and the nature of frequency deviations present in the system. If the inertia is
402 high and frequency fluctuations are caused by slow phenomena (as currently
403 happen), the performance of the BESSs is similar to that of fast turbine gover-
404 nors. As inertia decreases and more stochastic fast noises are present into the
405 grid (for example due to the increase of renewable sources) the BESSs are more
406 effective than the conventional primary frequency controllers of synchronous
407 machines (even more than doubling the performance of slow thermal plants).
408 Finally, variable droop control strategy does not seem to impact signal standard
409 deviation and just marginally modify the frequency stability with respect to the
410 fixed droop case, while at the same time improves the BESS SOC management.

411 Future work will be focused on a more rigorous assessment of the impact
412 of variable droop control discussed in the paper by considering more scenarios,
413 parameters and different regulation laws.

414 **Acknowledgment**

415 This work has been developed as part of the activities of RESERVE Euro-
 416 pean project, grant agreement No. 727481.

417 Federico Milano is funded by Science Foundation Ireland (SFI), through the
 418 Investigator Programme, under award AMPSAS, Grant No. SFI/15/IA/3074.
 419 The opinions, findings and conclusions or recommendations expressed in this
 420 material are those of the authors and do not necessarily reflect the views of the
 421 SFI.

422 The authors would like to thank Eng. Ferdinando Parma, Eng. Massimo
 423 Pozzi and Dr. Davide Falabretti for their help in this work.

424 **Appendix A. Grid static and dynamic characteristics**

Table A.5: Main elements of the transmission system used

Network	#	Loads and Power Plants	#
AC Power Lines	796	Loads	346
Bus	1479	Conventional Generators	22
Transformers	1055	Wind power plants	472

Table A.6: Parameters of primary and secondary frequency control

Primary Reserve Control	Band [MW]	Reserved [%]	Droop [%]	Deadband [mHz]
S1	421	10	5	15
S2 & S3	302	10	5	15

Table A.7: Parameters of the turbine governors of conventional generators

Time Constant	Steam	Hydro	Gas
T_1 [s]	10	2.5	0.5
T_2 [s]	3	0	0

425 **Appendix B. Noises parameters of the Scenarios**

Table B.8: Stochastic noises parameters values used to create the scenarios

Scenario #	Load		Wind	SSP1		SSP2	
	Δt_i	σ_{Load}	σ_w	Δt_{CG}	Δp_{max}	Δt_{CG}	Δp_{max}
	[s]	[%]	[%]	[min]	[MW]	[min]	[MW]
S1 (6:00-12:00)	0.5	2.75	2.5	3-6	33	13-50	50
S1 (12:00-18:00)	0.5	3	5	4-7	38	15-50	47.5
S2 (6:00-18:00)	0.5	8.5	12.5	3.5-6.5	39	14-50	22.5
S3 (6:00-18:00)	0.5	16	25	4-7	20	14-50	10

426 **Bibliography**

- 427 [1] Kempener R, Borden E. Battery storage for renewables: market status and
428 technology outlook. International Renewable Energy Agency, Abu Dhabi,
429 2015.
- 430 [2] ENTSO-E. Consultation Report "FCR Cooperation"; 2017.
- 431 [3] National Grid. National Grid frequency services,
432 [https://www.nationalgrideso.com/balancing-services/frequency-response-](https://www.nationalgrideso.com/balancing-services/frequency-response-services/enhanced-frequency-response-efr)
433 [services/enhanced-frequency-response-efr](https://www.nationalgrideso.com/balancing-services/frequency-response-services/enhanced-frequency-response-efr); 2019 [accessed 4 June 2019].

- 434 [4] Order no. 755: Frequency regulation compensation in the organized whole-
435 sale power markets. Federal Energy Regulatory Commission, Washington
436 DC, 2011.
- 437 [5] Ramírez M, Castellanos R, Calderón G, Malik O. Placement and sizing
438 of battery energy storage for primary frequency control in an isolated sec-
439 tion of the Mexican power system. *Elec Power Syst Res* 2018;160:142-150.
440 <https://doi.org/10.1016/j.epsr.2018.02.013>.
- 441 [6] ENTSO-E. Frequency stability evaluation criteria for the synchronous zone
442 of continental Europe; 2016.
- 443 [7] Ortega Á, Milano F. Modeling, simulation, and comparison of control tech-
444 niques for energy storage systems. *IEEE Trans Power Syst* 2017;32(3):2445-
445 54. <https://doi.org/10.1109/TPWRS.2016.2602211>.
- 446 [8] Ortega Á, Milano F. Stochastic transient stability analysis of transmission
447 systems with inclusion of energy storage devices. *IEEE Trans Power Syst*
448 2018;33(1):1077-79. <https://doi.org/10.1109/TPWRS.2017.2742400>.
- 449 [9] Toma L, Sanduleac M, Baltac SA, Arrigo F, Mazza A, Bompard E et al.
450 On the virtual inertia provision by BESS in low inertia power systems.
451 In: *IEEE International Energy Conference (ENERGYCON) 2018*, pp.1-6.
452 <https://doi.org/1109/ENERGYCON.2018.8398755>.
- 453 [10] Zhao H, Hong M, Lin W, Loparo KA. Voltage and frequency regulation
454 of microgrid with battery energy storage systems. *IEEE Trans Smart Grid*
455 2019;10(1):414-24.10. <https://doi.org/1109/TSG.2017.2741668>
- 456 [11] Aghamohammadi MR, Abdolahinia H. A new approach for opti-
457 mal sizing of battery energy storage system for primary frequency
458 control of islanded microgrid. *Int J Elec Power* 2014;54,325-33.
459 <https://doi.org/10.1016/j.ijepes.2013.07.005>.

- 460 [12] Oudalov A, Chartouni D, Ohler C. Optimizing a battery energy stor-
461 age system for primary frequency control. *IEEE Trans Power Syst* 2007;
462 22(3),1259–66. <https://doi.org/10.1109/TPWRS.2007.901459>.
- 463 [13] Thien T, Schweer D, vom Stein D, Moser A, Sauer D U. Real-world op-
464 erating strategy and sensitivity analysis of frequency containment reserve
465 provision with battery energy storage systems in the German market. *J.*
466 *Energy Storage* 2017;13:143-63. <https://doi.org/10.1016/j.est.2017.06.012>
- 467 [14] Brivio C, Mandelli S, Merlo M. Battery energy storage system for pri-
468 mary control reserve and energy arbitrage. *Sustainable Energy, Grids Netw*
469 2016;6:152–65. <https://doi.org/10.1016/j.segan.2016.03.004>.
- 470 [15] Zhang YJA, Zhao C, Tang W, Low SH. Profit-maximizing plan-
471 ning and control of battery energy storage systems for primary
472 frequency control. *IEEE Trans Smart Grid* 2016;9(2):712-23.
473 <https://doi.org/10.1109/TSG.2016.2562672>.
- 474 [16] Cheng B, Powell W B. Co-optimizing battery storage for the frequency
475 regulation and energy arbitrage using multi-scale dynamic programming.
476 *IEEE Trans Smart Grid* 2016;9(3):1997-2005.
- 477 [17] Engels J, Claessens B, Deconinck G. Combined stochastic optimization of
478 frequency control and self-consumption with a battery. *IEEE Trans Smart*
479 *Grid* 2017;10(2):1971-81.
- 480 [18] Namor E, Sossan F, Cherkaoui, R, Paolone M. Control of battery storage
481 systems for the simultaneous provision of multiple services. *IEEE Trans*
482 *Smart Grid* 2018;10(3):2799-808.
- 483 [19] Mégel J, Mathieu J L, Andersson G. Scheduling distributed energy storage
484 units to provide multiple services under forecast error. *Int J Elect Power*
485 *Energy Syst* 2015;72:48–57.

- 486 [20] Stein K, Tun M, Matsuura M, Rocheleau R. Characterization of a fast
487 battery energy storage system for primary frequency response. *Energies*
488 2018; 11(12) 3358. <https://doi.org/10.3390/en11123358>.
- 489 [21] Jo H, Choi J, Agyeman KA, Han S. Development of frequency con-
490 trol performance evaluation criteria of BESS for ancillary service: a
491 case study of frequency regulation by KEPCO. In: *IEE Innovative*
492 *Smart Grid Technologies-Asia Conference (ISGT-Asia) 2017*, pp.1-5.
493 <https://doi.org/10.1109/ISGT-Asia.2017.8378437>
- 494 [22] Cheng Y, Tabrizi M, Sahni M, Povedano A, Nichols D. Dy-
495 namic available AGC based approach for enhancing utility scale en-
496 ergy storage performance. *IEEE Trans Smart Grid* 2014;5(2):1070-78.
497 <https://doi.org/10.1109/TSG.2013.2289380>.
- 498 [23] Chen S, Zhang T, Gooi HB, Masiello RD, Katzenstein W. Penetration rate
499 and effectiveness studies of aggregated BESS for frequency regulation. *IEEE*
500 *Trans Smart*;7(1):167-77. <https://doi.org/10.1109/TSG.2015.2426017>.
- 501 [24] Zhang F, Hu Z, Xie X, Zhang J, Song J. Assessment of the ef-
502 fectiveness of energy storage resources in the frequency regulation
503 of a single-area power system. *IEEE Trans Power Syst*;32(5):3373-80.
504 <https://doi.org/10.1109/TPWRS.2017.2649579>.
- 505 [25] ENTSO-E, EURELECTRIC. *Deterministic frequency deviations—root*
506 *causes and proposals for potential solutions*; 2011.
- 507 [26] ENTSO-E. *Continental Europe Significant Frequency deviations*; 2011.
- 508 [27] Remppis S, Gutekunst F, Weissbach T, Maurer M. Influence of 15-minute
509 contracts on frequency deviations and on the demand for balancing energy.
510 In: *International ETG Congress 2015*, pp.1-7.
- 511 [28] Arrigo F, Merlo M, Parma F. Fourier transform based procedure
512 for investigations on the grid frequency signal. In: *Innovative Smart*

- 513 Grid Technologies Conference Europe (ISGT-Europe) 2017, pp.1-6.
514 <https://doi.org/10.1109/ISGTEurope.2017.8260312>.
- 515 [29] Anderson PM, Fouad AA. Power system control and stability. 2nd ed. John
516 Wiley & Sons; 2008.
- 517 [30] Milano F. Power System Modelling and Scripting. London:Springer; 2010.
- 518 [31] Zárata-Miñano R, Anghel M, Milano F. Continuous wind speed mod-
519 els based on stochastic differential equations. Appl Energy 2013;104:42-9.
520 <https://doi.org/10.1016/j.apenergy.2012.10.064>
- 521 [32] Milano F, Ortega Á. Converter-Interfaced Energy Storage Systems. Lon-
522 don: Cambridge University Press; 2019.
- 523 [33] Eirgrid. Irish Grid Code. [http://www.eirgridgroup.com/site-](http://www.eirgridgroup.com/site-files/library/EirGrid/GridCodeVersion6.pdf)
524 [files/library/EirGrid/GridCodeVersion6.pdf](http://www.eirgridgroup.com/site-files/library/EirGrid/GridCodeVersion6.pdf); 2015 [accessed 4 June
525 2019]
- 526 [34] Kundur P, Balu NJ, Lauby MG. Power system stability and control. New
527 York: McGraw-Hill; 1994.
- 528 [35] Mele FM, Ortega Á, Zárata-Miñano R, Milano F. Impact of variability, un-
529 certainty and frequency regulation on power system frequency distribution.
530 In: Power Systems Computation Conference (PSCC-Genoa) 2016, pp.1-6.
531 <https://doi.org/10.1109/PSCC.2016.7540970>
- 532 [36] Terna. Italian grid code, attachment A15: load frequency control partici-
533 pation, <https://download.terna.it/terna/0000/0105/32.pdf>; 2008 [accessed
534 4 June 2019]
- 535 [37] EirGrid and SONI. All-island ten year transmission forecast statement;
536 2017.
- 537 [38] Milano F. A Python-based software tool for power system analy-
538 sis. IEEE Power & Energy Society General Meeting 2013, pp.1-5.
539 <https://doi.org/10.1109/PESMG.2013.6672387>.



This Article is part of a project that has received funding from the **European Union's Horizon 2020 research and innovation programme** under grant agreement N°727481